The Impact of Weak CH ···Rh Interactions on the Structure and Reactivity of trans –[Rh(CO) 2 (phosphine) 2] + : An Experimental and Theoretical Examination

The Impact of Weak C−H⋯Rh Interactions on the Structure and Reactivity of *trans*-[Rh(CO)$_2$(phosphine)$_2$]$^+$: An Experimental and Theoretical Examination

Michael Montag,[a] **Irena Efremenko,**[a] **Revital Cohen,**[b] **Gregory Leitus,**[b] **Linda J. W. Shimon,**[b] **Yael Diskin-Posner,**[b] **Yehoshoa Ben-David,**[a] **Jan M. L. Martin,***[a] **and David Milstein***[a]

Abstract: The crystal structure of the new cationic Rh^I complex *trans*-[Rh(CO)$_2$(L)$_2$]BF$_4$ (L = α^2-(diisopropylphosphino)isodurene) was found to exhibit a nonlinear OC−Rh−CO fragment and weak intramolecular C−H⋯Rh interactions. These interactions, which have also been shown to occur in solution, have been examined by density functional theory calculations and found to be inextricably linked to the presence of the distorted OC−Rh−CO fragment. This linkage has also

Keywords: anagostic interaction · C−H activation · carbonyl ligands · phosphines · rhodium

been demonstrated by comparison with a highly similar Rh^I complex, in which these C−H⋯Rh interactions are absent. Furthermore, the presence of these weak interactions has been shown to have a significant effect on the reactivity of the metal center.

Introduction

The activation of strong carbon–hydrogen bonds is currently a topic of great interest,[1] especially with regards to the development of new synthetic methodologies for organic chemistry.[2] Recently, we described a cationic Rh^I PCP-type pincer system in which CO was found to promote the oxidative addition of a C−H bond,[3] rather than retard it as common experience would suggest.[4] This unexpected observation led us to investigate further aspects of C−H activation in the presence of CO.

In particular, both experimental and theoretical evidence suggested that C−H activation in the abovementioned pincer system involves an 18-electron trigonal-bipyramidal Rh^I intermediate, in which the equatorial positions are occupied by two CO ligands and a C−H bond (which later adds to the metal center) and the axial positions are occupied by phosphine donor groups from the pincer ligand.[3] This putative intermediate, which can be viewed as an adduct of the C−H bond with a distorted, "transoid" [Rh(CO)$_2$(phosphine)$_2$]$^+$ fragment, prompted us to explore the potential for C−H activation in nonchelated (nonpincer) systems, the overall structure of which resembles this fragment.

Herein we describe such a cationic *trans*-dicarbonyl bisphosphine Rh^I complex, which is based on the monophosphine ligand α^2-(diisopropylphosphino)isodurene (ligand **1**, Scheme 1a).[5] The crystal structure of this complex exhibits an intriguing relationship between bent CO ligands and weak intramolecular C−H⋯Rh interactions, which are also shown to have a significant impact on the reactivity of this system in solution. Furthermore, a detailed theoretical examination of this system reveals the electronic origin of these unique structural features and their strong interdependence. This, in turn, sheds light on the potential role of CO in the activation of strong C−H bonds, and also on the important role of weak C−H⋯Rh interactions.

[a] M. Montag, Dr. I. Efremenko, Y. Ben-David, Prof. J. M. L. Martin, Prof. D. Milstein
Department of Organic Chemistry
Weizmann Institute of Science
Rehovot 76000 (Israel)
Fax: (+972) 8-934-4142
E-mail: gershom@weizmann.ac.il
        david.milstein@weizmann.ac.il

[b] Dr. R. Cohen, Dr. G. Leitus, Dr. L. J. W. Shimon, Dr. Y. Diskin-Posner
Department of Chemical Research Support
Weizmann Institute of Science
Rehovot 76000 (Israel)

Supporting information for this article (*xyz* coordinates of the calculated complexes) is available on the WWW under http://dx.doi.org/10.1002/chem.200801171 or from the authors.
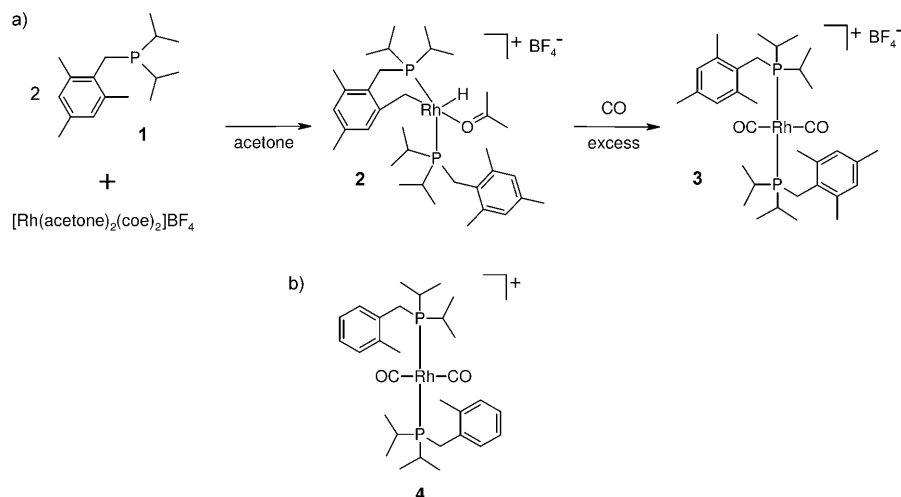
Scheme 1. a) Preparation of complex **3**, and b) model system **4**, which was used for the density functional theory (DFT) analysis of **3**.

least several hours. Nonetheless, the unique structural features of **3** were only revealed by examination of its crystal structure.

Molecular structure of complex 3—a transoid species with a nonlinear Rh(CO)₂ fragment and C−H···Rh interactions: Crystals of **3** suitable for X-ray diffraction were coincidentally obtained when a dioxane solution of the complex was heated at 95 °C for 90 minutes. The crystal structure parameters are given in Table 1. As expected, the complex, which

Results and Discussion

Preparation of a cationic *trans*-dicarbonyl bisphosphine Rh^{I} complex of ligand 1: In an attempt to prepare a cationic *trans*-dicarbonyl bisphosphine Rh^{I} complex that may be utilized to emulate the abovementioned C−H activation intermediate, we chose to use monophosphine ligand **1** (Scheme 1a). The reasons for choosing this ligand are twofold. First, the phosphine donor group in **1** has one benzyl and two isopropyl substituents, which makes it essentially identical, both sterically and electronically, to the phosphine donors of the abovementioned PCP ligand, which has been shown to undergo CO-promoted C−H oxidative addition.[3] Second, previous work has shown that reaction of two equivalents of ligand **1** with the Rh^{I} precursor [Rh-(acetone)₂(coe)₂]BF₄ (coe = cyclooctene), as shown in Scheme 1a, leads to the cyclometalated Rh^{III} complex **2**,[5c] the very structure of which, with its *trans*-positioned phosphine moieties, makes it a potential precursor for the preparation of a cationic *trans*-dicarbonyl bisphosphine Rh^{I} complex. Indeed, we have found that when complex **2** is treated with excess CO, facile C−H reductive elimination takes places to afford the cationic *trans*-dicarbonyl bisphosphine Rh^{I} complex **3** (Scheme 1a).[6]

A solution of **3** in CDCl₃ exhibits a doublet at $\delta = 55.87$ ppm ($^{1}J(\mathrm{Rh,P}) = 103.6$ Hz) in the $^{31}\mathrm{P}\{^{1}\mathrm{H}\}$ NMR spectrum, and its relatively simple $^{1}\mathrm{H}$ NMR spectrum (see the Experimental Section) supports a highly symmetrical structure with no cyclometalation. Furthermore, the $^{19}\mathrm{F}\{^{1}\mathrm{H}\}$ NMR spectrum of this solution features a sharp singlet at $\delta = -154.77$ ppm, which is consistent with a noncoordinated, outer-sphere BF₄⁻ counterion. The IR spectrum of **3** (nujol mull) features a strong asymmetric CO stretch band at $\tilde{\nu} = 2008$ cm⁻¹, which is consistent with a *trans* configuration for the carbonyl ligands. It is also worth noting that **3** was found to be air-stable at least for several days, both in solution and in the solid state, and vacuum-stable for at

Table 1. Crystallographic data for *anti*-**3**, *syn*-**3**, and **6**.

	anti-**3**	*syn*-**3**	**6**
formula	C₃₄H₅₄BF₄-O₂P₂Rh	C₃₄H₅₄BF₄-O₂P₂Rh·CH₂Cl₂	C₂₈H₄₂BF₄-O₂P₂Rh
M_{r}	746.43	831.36	662.28
space group	$P\bar{1}$	$P2_{1}/n$	$Pbcn$
crystal system	triclinic	monoclinic	orthorhombic
a [Å]	11.147(2)	17.910(4)	15.9798(4)
b [Å]	12.297(3)	12.378(3)	11.6684(2)
c [Å]	14.554(3)	19.731(4)	16.5021(3)
α [°]	100.71(3)	90.0	90.0
β [°]	107.37(3)	112.68(3)	90.0
γ [°]	99.82(3)	90.0	90.0
V [Å³]	1815.7(6)	4036(1)	3076.96(11)
Z	2	4	4
ρ_{calcd} [g cm⁻³]	1.365	1.368	1.430
μ [mm⁻¹]	0.607	0.682	0.707
T [K]	120(2)	120(2)	120(2)
R_{1} [$I > 2\sigma(I)$] [%]	2.82	4.20	3.48
R_{1} (all data) [%]	3.34	5.70	8.44

crystallized in the $P\bar{1}$ space group, exhibited a tetracoordinate rhodium center bound to two molecules of **1** and two CO ligands (Figure 1), with a *trans*-dicarbonyl bisphosphine configuration[7] and an outer-sphere BF₄⁻ counterion. The arene moieties of the phosphine ligands were found to point in opposite directions on either side of the metal center (*anti* configuration). However, unlike the few reported crystal structures of cationic *trans*-dicarbonyl bisphosphine Rh^{I} complexes,[8] all of which have a nearly perfect square-planar geometry, complex **3** was found to exhibit a significantly distorted coordination geometry.

The most prominent structural feature of **3** is the OC−Rh−CO fragment, which deviates considerably from linearity, with a C1-Rh1-C2 angle of 166.31(8)°.[9] Moreover, one of the CO ligands is also significantly bent with respect to the metal center, with a Rh1-C2-O2 angle of 172.83(17)°, whereas the second Rh−CO fragment is virtually linear
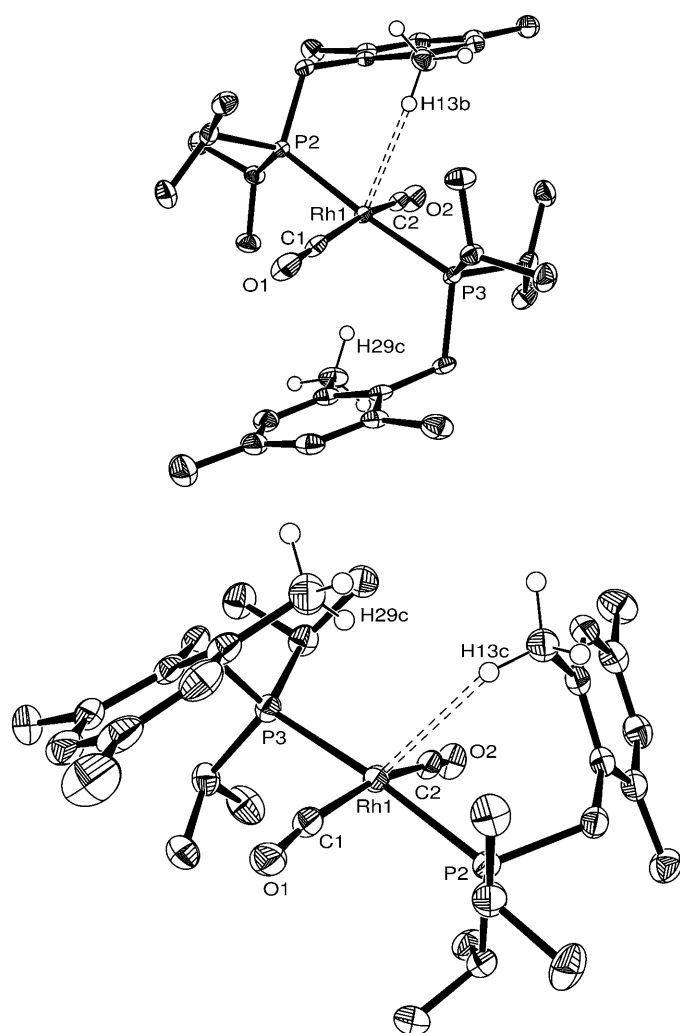
Figure 1. Crystal structures of the *anti* (top) and *syn* (bottom) conformers of **3**, with ellipsoids drawn at the 50% probability level. All hydrogen atoms (except for those on C13 and C29), solvent molecules, and BF₄⁻ counterions were omitted for clarity.

1.924(2) Å) as compared with other reported rhodium carbonyl complexes,[12] whereas the C−O bonds are relatively short (C1−O1 = 1.129(2) Å, C2−O2 = 1.132(2) Å) and very close in length to free CO (1.1283 Å).[13] The geometrical data related to the primary coordination sphere of **3** are compiled in Table 2.

Another important attribute of the molecular structure of **3**, which became apparent from the crystal data, is the existence of short contacts between the metal center and neighboring arene methyl groups.[14] The interatomic distances associated with these contacts are Rh1−C13 = 3.469(2) Å and Rh1−H13b = 2.55(3) Å for the first methyl group, and Rh1−C29 = 3.680(2) Å and Rh1−H29c = 2.80(2) Å for the second methyl group (hydrogen atoms were located in the electron-density map and their positions were freely refined). From these interatomic distances, it is possible to draw two important conclusions relating to the structure of **3**. First, it can be clearly seen that the two interacting methyl moieties are positioned nonsymmetrically with respect to the metal center, with one methyl group (C13) being closer to rhodium than the other. Moreover, the hydrogen atom from the proximal methyl group (H13b) is located at the vertex of the C1-Rh1-C2 angle, which implies a possible link between the short C−H···Rh contact and the nonlinear coordination of the carbonyl ligands (see below). Second, the Rh···H distances found for both methyl groups are characteristic of weak C−H···metal interactions, known as "anagostic" interactions.[15] This type of interaction has been previously discussed in the literature,[16] and refers to any M−H−C interaction that does not involve a three-center, two-electron bond, which is a characteristic of agostic interactions.[15]

The existence of anagostic interactions in solution is usually evident from downfield shifts of the ¹H NMR spectroscopic signals associated with the interacting hydrogen atoms, whereas agostic interactions lead to upfield shifts,[16f] but in the present case no significant signal shifts were observed, even at low temperatures (e.g., −55 °C). Nonethe-

(179.18(16)°). It is worth noting that the deviations from linearity observed for **3** are quite uncommon among all known carbonyl complexes,[10] and are even more unusual among rhodium complexes.[11] The P−Rh−P fragment also deviates from linearity, but to a lesser extent, with a P2-Rh1-P3 angle of 175.014(16)°. Overall, the coordination geometry of **3** resembles a flattened tetrahedron. As for the bond lengths associated with the CO ligands, the Rh−CO bonds are relatively long (Rh1−C1 = 1.915(2) Å, Rh1−C2 =

Table 2. Selected bond lengths [Å] and angles [°] for **3** and **6** and their computed analogues.

	anti-**3** (exptl)	*anti*-**4** (calcd)	*syn*-**3** (exptl)	*syn*-**4** (calcd)	**6**[a] (exptl)	**6**[a] (calcd)
Rh1−C1	1.915(2)	1.910	1.913(3)	1.899	1.913(3)	1.913
Rh1−C2	1.924(2)	1.915	1.926(3)	1.902	–	–
C1−O1	1.129(2)	1.138	1.131(3)	1.141	1.129(4)	1.138
C2−O2	1.132(2)	1.138	1.133(3)	1.141	–	–
Rh1−P2	2.3626(10)	2.375	2.3498(9)	2.371	2.3489(5)	2.371
Rh1−P3	2.3699(11)	2.376	2.3548(8)	2.378	–	–
Rh1···C[b]	3.469(2)	3.639	3.484(3)	3.686	3.536(3)	3.678
C[b]−H[b]	0.99(2)	1.102	0.97(4)	1.102	0.94(3)	1.090
Rh1···H[b]	2.55(3)	2.674	2.65(4)	2.752	3.13(3)	3.405
Rh1···C29	3.680(2)	3.763	3.755(4)	3.699	–	–
C29−H29c	1.01(2)	1.100	0.93(3)	1.102	–	–
Rh1···H29c	2.80(2)	2.799	2.98(3)	2.747	–	–
C1-Rh1-C2	166.31(8)	168.82	164.70(11)	148.84	180.0	180.0
Rh1-C1-O1	179.18(16)	178.95	171.9(2)	166.93	177.81(18)	177.2
Rh1-C2-O2	172.83(17)	173.48	172.3(2)	166.29	–	–
P2-Rh1-P[c]	175.014(16)	176.29	173.88(2)	175.41	180.0	180.0

[a] Complex **6** is centrosymmetric and therefore duplicate values were omitted. [b] C13 and H13b for *anti*-**3**, C13 and H13c for *syn*-**3**, C6 and H6 for **6**. [c] P3 for *anti*- and *syn*-**3**, P2a for **6**.

less, we found that when **3** was dissolved in CD_3OD and warmed at 80°C for several days, under excess CO to prevent decomposition,[17] selective H/D exchange took place between the solvent and the two arene methyl groups positioned *ortho* to the methylene bridges of both phosphine ligands, whereas the methyl groups in the *para* positions remained unaffected.[18] This chemical exchange supports the existence of C−H⋯Rh interactions, which are expected to enhance the acidity of the alkyl C−H bonds.[19]

The observation of nonlinearly coordinated CO ligands and anagostic interactions in **3**, and their possible interrelation, prompted us to examine the system in greater detail. Therefore, we analyzed two additional crystals of **3** that were grown under different conditions to insure the reproducibility of the above observations. The first crystal, grown in cold (−20°C) THF overlaid with pentane, gave a molecular structure that was virtually identical to that described above (including the Rh⋯H bond lengths; see the Experimental Section for crystal data).[20,21] However, the second crystal, which was grown from a CH_2Cl_2 solution overlaid with diethyl ether (also at −20°C; see Table 1 for the crystal structure parameters), revealed a rather different picture (Figure 1). In this case, the complex, which crystallized in the $P2_1/n$ space group, was found to have a different spatial arrangement of the phosphine ligands about the metal center, such that both arene moieties reside on the same side of the metal center (*syn* configuration). Nonetheless, this new structure, which constitutes a different conformer of **3**, was found to have a coordination sphere very similar to that of the *anti* conformer (see Table 2). Thus, the *syn* conformer (*syn*-**3**) has a markedly nonlinear OC−Rh−CO fragment ($\sphericalangle$C1-Rh1-C2 = 164.70(11)°, $\sphericalangle$Rh1-C1-O1 = 171.9(2)°, and $\sphericalangle$Rh1-C2-O2 = 172.3(2)°), as well as short contacts between the metal center and neighboring arene methyl groups (Rh1−C13 = 3.484(3) Å, Rh1−H13c = 2.65(4) Å, and Rh1−H29c = 2.98(3) Å).[22] The P−Rh−P fragment is also nonlinear ($\sphericalangle$P2-Rh1-P3 = 173.88(2)°), but its angle vertex points in the opposite direction to that of *anti*-**3**, such that the overall coordination geometry resembles a flattened square pyramid, rather than a flattened tetrahedron. Furthermore, the bond lengths associated with the CO ligands in *syn*-**3** (Rh1−C1 = 1.913(3) Å, Rh1−C2 = 1.926(3) Å, C1−O1 = 1.131(3) Å, and C2−O2 = 1.133(3) Å) are virtually identical to those of *anti*-**3**.[23] Therefore, it can be concluded that both the distorted geometry of **3** and the C−H⋯Rh interactions are inherent attributes of this complex in the solid state (and perhaps also in solution), and are probably not a result of artifacts or measurement errors. Furthermore, it appears that these geometry distortions do not originate from crystal packing forces or intramolecular steric repulsions because these structural characteristics recur in different crystal and intramolecular environments. This conclusion was corroborated by a theoretical examination, as described below.

Theoretical examination of the structural and electronic properties of 3: In an attempt to better understand the ob-

servations described above, we carried out a DFT investigation of **3** (see the Experimental Section for the computational details). In the interest of computational simplicity, the calculations were run with model system **4** (Scheme 1b), which is a simplified analogue of **3** that has only those arene methyl groups which are directly involved in the C−H⋯Rh interactions. The BF_4^- counterion was not included in these calculations because there was no evidence for its coordination to the metal center of **3**, either in the crystal structure or in solution (see above). The calculations, which were performed at the PBE0/pc-1 level of theory, found the *anti* and *syn* conformers of **4** to be quite close in energy, with the *anti* conformer being 3.28 kcal mol^{-1} more stable than *syn*. The optimized structures of *anti*- and *syn*-**4** were found to closely reproduce the experimental geometries of the respective conformers of **3**, including the angles and bond lengths associated with the CO ligands[24] and the C−H⋯Rh distances.[25] The optimized geometrical data are presented in Table 2 alongside the observed values. It is important to note that the generally high similarity between the experimental and calculated (gas phase) structures supports the conclusion that the observed distortions in the OC−Rh−CO fragment are not the result of crystal packing forces, as mentioned above.

Analysis of the electronic structure of the two conformers of **4** indicated that the main contribution to the Rh⋯H bonding comes from C−H→Rh electron donation. This is clearly apparent from the molecular orbitals of the two conformers, which exhibit an overlap between Rh $4d_{z^2}$ and σ_{C-H}.[26] This electron donation leads to slight elongation of the C−H bond (1.102 Å in both conformers), as compared with the other methyl C−H bonds in **4** (1.095–1.098 Å), and it also accounts for the increased acidity of the C−H bond, as observed in the H/D exchange experiment described above for **3**. More importantly, however, our calculations revealed an intimate link between the C-Rh-C angle and the anagostic interaction. It was found that deviation of the C-Rh-C angle from linearity enhances the Lewis acidity of the metal center along the *z* axis in the direction of the interacting C−H bond (Figure 2). This effect is due to a decrease in CO→Rh σ donation, as a result of a reduction in the overlap between the CO 5σ and Rh $4d_{z^2}$ orbitals (Figure 2a), and also to the emergence of new Rh→CO π back-donations that involve the metal d_{z^2} and d_{yz} orbitals and the two CO 2π* orbitals (Figure 2b). The interaction between π* and the d_{z^2} orbital is also responsible for the bent Rh-C-O angles because this bending enhances orbital overlap.

Facile distortion of tetracoordinate d^8 carbonyl complexes from the common square-planar geometry, without the effect of additional ligands, has been predicted by Hoffmann and Elian based on qualitative extended Hückel analysis.[27] However, further work by Hoffmann and co-workers has demonstrated that whereas this prediction holds for neutral complexes, positively charged complexes with strongly donating ligands should actually favor square-planar geometry.[28] This difference in structure was linked to the lower d orbital energies of cationic metals relative to neutral ones
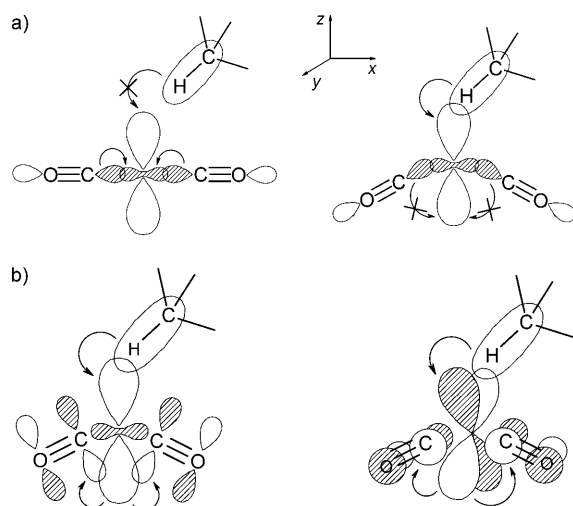
Figure 2. Critical orbital interactions responsible for the anagostic bonding. a) Bending-induced changes in the σ system. In the linear complex (left), the CO→Rh σ donation hinders the anagostic interaction by hampering the σ_{C-H}→Rh electron donation; in the bent complex (right) the CO→Rh σ donation is itself hampered, thereby allowing the σ_{C-H}→Rh electron donation. b) Bending-induced, anagostic-enhancing interactions in the π system (left: d_{z^2}→π*; right: d_{yz}→π*).

Figure 3. Effect of ∢C-Rh-C bending on a) the relative energies of the calculated structures $[Rh(CO)_2(PH_3)_2]^+$, $[Rh(CH_4)(CO)_2(PH_3)_2]^+$, and $[Rh(CH_4)(CO)_2(PMe_3)_2]^+$, and b) on the optimized Rh⋯H distance in the methane complexes.

(e.g., Rh⁺ versus Ru⁰), making the former more electronegative (i.e., a better σ acceptor and worse π donor) with respect to CO. More recent work by Eisenstein, Caulton and co-workers has focused on a neutral d⁸ Ru⁰ complex, *trans*-[Ru(CO)₂(P*t*Bu₂Me)₂],[29] in which the coordination sphere is very similar to that of **3**. As predicted by Hoffmann and co-workers, this complex exhibits a sawhorse structure with a remarkably acute C-Ru-C angle of 133.3(4)°,[30] in marked distinction from **3**. By using ab initio methods (HF/MP2 level), Eisenstein, Caulton, and co-workers demonstrated that a model system, *trans*-[Ru(CO)₂(PH₃)₂], adopts a sawhorse geometry that is nearly identical to the experimental system.[29] Furthermore, they showed that bending of the OC−Ru−CO fragment is essential for the stabilization of this complex because it increases π back-donation from both d_{z^2} and d_{yz} to CO and diminishes the destabilizing σ donation from CO to d_{z^2}.[31] The authors also compared this system with an isoelectronic Rh^I model system, *trans*-[Rh(CO)₂(PH₃)₂]⁺,[29] which is of relevance to the current work. This system was found to adopt a square-planar geometry, in agreement with essentially all experimental structures,[6] and to be destabilized by bending of the OC−Rh−CO fragment. However, the authors did not provide a detailed examination of the effect of C-Rh-C angle variation on the energetics of the system, and did not explore the influence of additional ligands, such as the anagostic C−H bond in the present case.

We examined the effect of C−Rh−C bending on the energy of *trans*-[Rh(CO)₂(PH₃)₂]⁺ at the PBE0/SDD level of theory, and found the potential energy surface to be rather flat, with a rise of only 2.38 kcal mol⁻¹ upon reducing ∢C-Rh-C from 180 to 150° (Figure 3a). The Walsh diagram
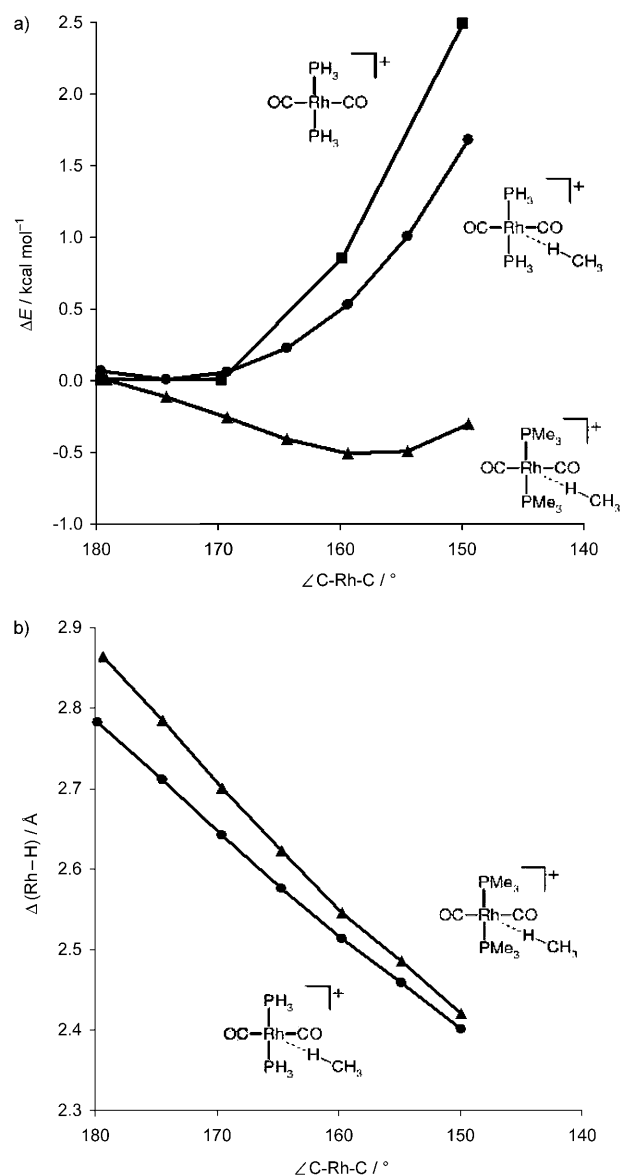
for this system (Figure 4) indicates that this rise in energy is due to destabilization of the b₂ orbital (d_{xz}), which is associated with the Rh→CO π back-donation, and is partly compensated by stabilization of the a₁ orbital (d_{z^2}), which is the main participant in the anagostic interaction. Nonetheless, it is clear that relatively little energy is required to bend the OC−Rh−CO fragment, and this energy can potentially be provided by the anagostic interaction, as observed in **3** and **4**. To examine this crucial point, we carried out DFT calculations on the model system *trans*-[Rh(CH₄)(CO)₂(PH₃)₂]⁺, which is an adduct of *trans*-[Rh(CO)₂(PH₃)₂]⁺ with methane in the axial position. Our calculations showed that the C−H⋯Rh interaction indeed lowers the energy cost of bending (e.g., only 1.62 kcal mol⁻¹ for ∢C-Rh-C = 150°; Figure 3a),
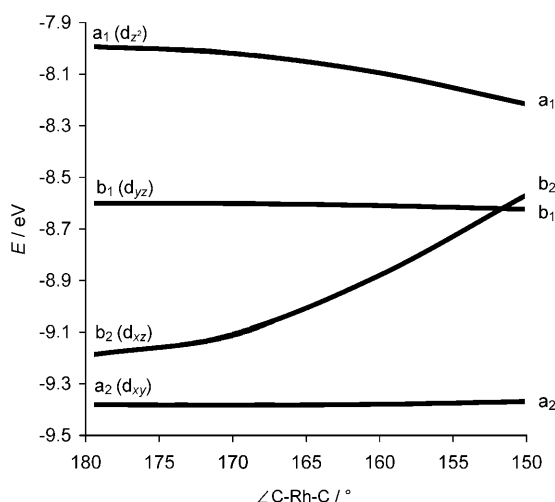
Figure 4. Walsh diagram showing the effect of ∡C-Rh-C bending on the energies of the calculated valence orbitals of [Rh(CO)$_2$(PH$_3$)$_2$]$^+$.

and even leads to a global energy minimum at ∡C-Rh-C ≈ 175°. Replacing PH$_3$ by the stronger donor PMe$_3$ leads to an even greater stabilization of the bent structures relative to the linear one, with a global minimum at ∡C-Rh-C ≈ 160°. This result is in good agreement with the observed geometries of **3** (∡C-Rh-C ≈ 165–166°), and thus strongly supports the conclusion that the distorted OC−Rh−CO fragment observed for this complex is due to electronic factors rather than steric repulsions.[32] Furthermore, it was found that the optimized Rh···H distances decrease with decreasing C-Rh-C angle (Figure 3b), which reflects stronger anagostic interactions as the angle becomes more acute. Note that the Rh···H distances in the more electron-rich PMe$_3$ complex are slightly longer than for the PH$_3$ complex, which supports the conclusion that the anagostic interaction is driven by C−H→Rh electron donation rather than electrostatic interactions,[33] contrary to the conclusions of previous theoretical studies on other systems.[16f] All in all, the DFT calculations clearly demonstrate that bending of the OC−Rh−CO fragment and the anagostic interaction are mutually stabilizing, which is in agreement with the observed structures of **3**. Furthermore, the low energies involved in both the anagostic interaction and C-Rh-C bending can account for the simple NMR spectra observed for **3** in solution, which are otherwise inconsistent with the asymmetric crystal structure.[34]

Effect of anagostic interactions on structure and reactivity— a comparative study: The anagostic interactions described above and the structural motifs that were found to be associated with them prompted us to examine additional types of such C−H···Rh interactions. Because the above observations involved alkyl sp^3 C−H bonds, we chose to extend the investigation to sp^2 C−H bonds. To this end, we replaced ligand **1** with a close analogue, ligand **5** (Scheme 2), which has a phenyl rather than mesityl arene moiety, such that only sp^2 C−H bonds were present. Thus, as shown in
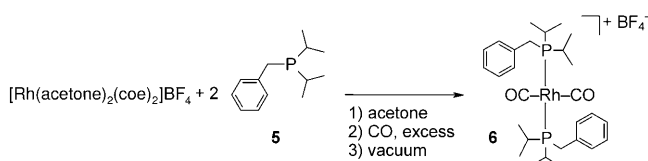
Scheme 2. Preparation of complex **6**.

Scheme 2, two equivalents of ligand **5** were reacted with [Rh(acetone)$_2$(coe)$_2$]BF$_4$ in acetone at room temperature, and the resulting solution was then treated with excess CO. After removal of the excess CO under vacuum, the product, complex **6**, was obtained in high yield.

The ^{31}P{^{1}H} NMR spectrum of **6** in CDCl$_3$ exhibits a doublet at $\delta = 51.21$ ppm ($^1J(\mathrm{Rh,P}) = 102.9$ Hz), which is very similar to the NMR signal observed for **3** ($\delta = 55.87$ ppm, $^1J(\mathrm{Rh,P}) = 103.6$ Hz), as expected in light of their similar structures. Furthermore, as in the case of **3**, complex **6** exhibits a simple ^{1}H NMR spectrum (see the Experimental Section), which is compatible with a symmetrical, noncyclometalated structure, and an IR spectrum that features a strong asymmetric CO stretch band at $\tilde{\nu} = 2015$ cm^{-1}, which is consistent with a *trans* configuration for the carbonyl ligands. Complex **6** was found to be stable under vacuum for at least several hours, as was also observed for **3**, but partly decomposed in air after a few days, in contrast to **3**.

Crystals of **6** that were suitable for X-ray diffraction were grown at −20°C from two solvent mixtures, namely, dichloromethane overlaid with pentane and methanol overlaid with diethyl ether. Both sets of conditions yielded practically identical crystals and molecular structures of **6** (see Table 1 and the Experimental Section). This complex, which crystallized in the *Pbcn* space group, has a molecular structure that is superficially similar to that of *anti*-**3**, as shown in Figure 5, with the arene moieties situated on either side of the metal atom, which is located at the center of a square-planar coor-
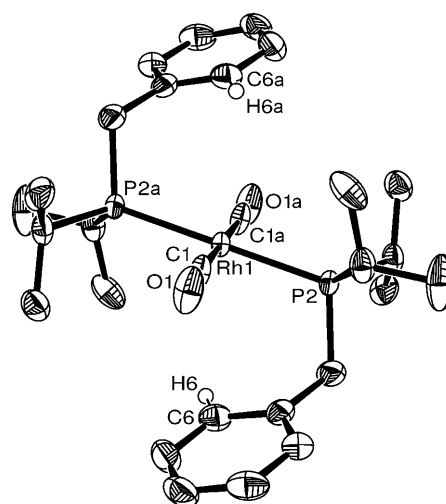

Figure 5. Crystal structure of **6**, with ellipsoids drawn at the 50% probability level. All hydrogen atoms (except for H6 and H6a) and the BF$_4^-$ counterion were omitted for clarity.

dination arrangement. However, closer examination of the coordination sphere in **6** reveals marked differences compared with that of **3**. One such difference is the absence of any significant anagostic interaction in the crystal structure of **6** because all of the Rh···H distances in this complex, including those associated with the arene C–H bonds, are longer than the upper limit set for anagostic interactions (i.e., Rh···H > 2.9 Å).[15,35] The absence of these interactions in **6** is probably due to steric hindrance, since an arene ring from one of the phosphine ligands would have to approach the metal center closely to allow for C–H···Rh interactions, and would thereby clash with the isopropyl groups of the second phosphine ligand. In complex **3**, on the other hand, the arene ring is kept safely away from the metal center (and neighboring isopropyl groups), whereas the protruding methyl moiety interacts with it.

Another significant difference between the crystal structures of **3** and **6** is the geometry of their primary coordination sphere. Whereas complex **3** features a markedly distorted coordination geometry (see above), complex **6** exhibits a virtually perfect square-planar arrangement (see Table 2), which is consistent with its centrosymmetric molecular structure (C_i point group, with the inversion center at rhodium). Of particular relevance to the current discussion is the fact that the OC–Rh–CO fragment in the crystal structure of **6** is practically linear (∡C1-Rh1-C1a = 180.0°[36] and ∡Rh1-C1-O1 = ∡Rh1-C1a-O1a = 177.81(18)°), which is in agreement with previously reported crystal structures of *trans*-dicarbonyl bisphosphine Rh^I complexes,[8] but in clear contrast to **3**, in which the two conformers have significantly distorted OC–Rh–CO fragments. It is worth noting that the bond lengths associated with the CO ligands in **6** (i.e., Rh–C and C–O) are practically identical to those in **3** (see Table 2).

The structure of **6** was also investigated by using gas-phase DFT calculations at the PBE0/pc-1 level of theory, as was also done for **3**. The BF$_4^-$ counterion was excluded since it is in the outer sphere in the crystal structure. The exact chemical composition of **6** was employed in the calculation, since no structural simplification was necessary, in contrast to **3**. These calculations were found to closely reproduce the crystal structure of **6** (see Table 2), including the linear OC–Rh–CO fragment and the absence of anagostic interactions, and this indicates that the configuration adopted by **6** in the crystal is not the result of packing forces, but is inherent in its molecular structure.

Further examination of **6** revealed that not only does it differ from **3** in its structural properties, but also in its chemistry. In contrast with **3**, which exhibited no observable BF$_4^-$ coordination when dissolved in chloroform, as was evident from the sharp, well-defined BF$_4^-$ signal in its room temperature ^{19}F{^{1}H} NMR spectrum (see above), complex **6** was found to coordinate this counterion under the same conditions, as was evident from the appearance of a very broad BF$_4^-$ signal (singlet at $\delta = -153.60$ ppm). The fact that **6** coordinates BF$_4^-$ in solution, whereas **3** does not (or does so very weakly), lends further weight to the role of anagostic interactions. In the absence of these interactions, the pri-

mary coordination spheres of the two complexes are identical and the arene moieties of the monophosphine ligands are not expected to exert significant steric influence on the metal center (because they are kept away by a flexible methylene bridge), and therefore, the two complexes should bind BF$_4^-$ with very similar, if not identical, affinities. Hence, the observation that **6** binds BF$_4^-$ in solution, whereas no such binding is observed for **3**, further supports the conclusion that **3** exhibits intramolecular anagostic interactions that shield the metal center from binding additional ligands, whereas **6** exhibits no significant anagostic interactions (as observed in the crystal structure).

Further, perhaps more striking, evidence for the effect of anagostic interactions on the coordination chemistry of the rhodium center was obtained when **3** and **6** were exposed to CO. As described above, the H/D exchange experiment conducted with **3** was carried out in CD$_3$OD under excess CO, to prevent the decomposition of the complex. ^{31}P and ^{1}H NMR spectra of this solution, taken before and after the addition of CO, indicated no observable changes in **3**. The same result was obtained when a solution of **3** in either CDCl$_3$ or CD$_2$Cl$_2$ was examined under excess CO at various temperatures (room temperature in both solvents, -40°C in CD$_2$Cl$_2$, and $+60$°C in CDCl$_3$). On the other hand, when complex **6** was dissolved in CD$_3$OD and treated with excess CO at room temperature, it was observed to fully convert to a new complex.[37] The new complex gave rise to a sharp doublet at $\delta = 63.30$ ppm (^1J(Rh,P) = 72.6 Hz) in the ^{31}P{^{1}H} NMR spectrum, which is clearly distinct from the broad doublet at $\delta = 52.23$ ppm (^1J(Rh,P) = 103.3 Hz) observed for **6** in CD$_3$OD. Furthermore, the IR spectrum of the new complex in solution in CH$_2$Cl$_2$ featured two strong CO stretching bands of roughly equal intensity at $\tilde{\nu} = 2008$ and 2024 cm^{-1}. Full characterization of this complex, including the use of ^{13}C-labeled CO (see the Experimental Section), ultimately revealed it to be tricarbonyl Rh^I complex **7** (Scheme 3), which is simply an adduct of **6** with an additional CO ligand. Such cationic Rh^I tricarbonyl bisphosphine complexes have been reported in the literature.[38]
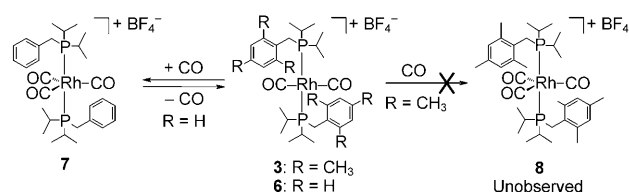
Scheme 3. Addition of CO to complexes **3** and **6**.

Complex **7** was found to be stable in solution at room temperature, but only under excess CO, since purging the solution with argon, or evaporating the solvent under vacuum, was found to lead to the loss of one CO ligand and regeneration of **6**.[39] Nevertheless, the fact that the reaction of **6** with CO afforded **7** in essentially quantitative yield, whereas complex **3** showed no observable reaction with CO

under the same conditions (i.e., complex **8** was never observed; see Scheme 3), lends strong support to the role of anagostic interactions in hindering the coordination of incoming CO molecules. As for the possibility that the difference in CO coordination between **3** and **6** arises from differences in the steric bulk of their arene moieties, our results regarding BF_4^- coordination have already shown this to be unlikely, and because CO is much smaller than BF_4^-, the possibility for such steric effects in the case of CO is even less likely. Moreover, Nurnberg and Werner have reported on the room-temperature preparation and isolation of the complex $[Rh(CO)_3(PiPr_3)_2]PF_6$,[8b] in which the triisopropylphosphine ligands are clearly more sterically demanding than ligand **1** in complex **3**.

Conclusion

Herein we have described a *trans*-dicarbonyl bisphosphine Rh^I complex, **3**, the crystal structures of which (*syn* and *anti* conformers) were found to exhibit both nonlinear OC−Rh−CO fragments and intramolecular C−H···Rh anagostic interactions that involve arene methyl groups (from phosphine ligand **1**). This complex was also found to undergo selective H/D exchange in solution, which involved only the arene methyl groups positioned *ortho* to the methylene bridges, thereby demonstrating that the anagostic interactions also occur in solution. DFT calculations traced these unique observations to bending-induced changes in the overlap between the orbitals of rhodium and the CO ligands. Thus, the occupied σ orbital of CO and the occupied metal d_{z^2} orbital show decreased overlap, whereas the empty π* orbitals of the CO ligands and the occupied metal d_{z^2} and d_{yz} orbitals exhibit increased overlap. Overall, these changes result in diminished electron density in orbitals d_{z^2} and d_{yz}, which renders them electron withdrawing. This, in turn, increases the electron-accepting ability of the metal center in the *z* direction, along which the relatively weak methyl C−H donor is situated, and the resulting anagostic interaction compensates for the energy cost of bending the otherwise linear OC−Rh−CO fragment.

Furthermore, we have prepared a second complex, **6**, the primary coordination sphere of which is identical to that of **3**, but its phosphine ligands (**5**) have no arene methyl groups. In contrast with **3**, the crystal structure of **6** was found to exhibit a virtually linear OC−Rh−CO fragment and no anagostic interactions. Moreover, we have observed that in solution **6** binds both its BF_4^- counterion and an additional CO molecule, whereas **3** does not, and this lends further support to the existence of anagostic interactions in **3** in solution. This also stresses the significance of anagostic interactions, which despite being relatively weak can have significant effects on the reactivity of a metal center.

All in all, the results described herein demonstrate a strong correlation between C−H···Rh anagostic interactions and the nonlinearity of carbonyl ligands. Therefore, these results are of great relevance to the topic of C−H bond activa-

tion, as they demonstrate the potential for promoting such reactions by fine-tuning the coordination geometry associated with strongly π-accepting ligands, such as CO and its isoelectronic congeners NO^+ and isonitriles.

Experimental Section

General procedures: All experiments with metal complexes and phosphine ligands were carried out under an atmosphere of purified argon in an MBraun Unilab glove-box. The complex $[Rh(acetone)_2(coe)_2]BF_4$ was prepared according to a literature procedure with appropriate modifications.[40] Ligand **1**,[5c] complex **2**,[5c] and ligand **5**[41] were prepared according to previously reported procedures. All solvents were reagent grade or better. All nondeuterated solvents were heated at reflux over sodium/benzophenone ketyl and distilled under argon. Deuterated solvents were used as received. All solvents were degassed with argon and kept in the glove-box over 3–4 Å molecular sieves (except for acetone, which was dried with Drierite). Commercially available reagents were used as received. Crystal structures were drawn by using the program ORTEP-3.[42]

Analysis: NMR spectra (^{1}H, ^{13}C, ^{19}F, and ^{31}P) were recorded by using Bruker Avance-400 and Bruker Avance-500 NMR spectrometers. All measurements were performed at 20°C unless otherwise noted. ^{1}H and ^{13}C NMR spectroscopic chemical shifts are reported in ppm relative to tetramethylsilane. ^{1}H NMR spectroscopic chemical shifts are referenced to the residual hydrogen signal of the deuterated solvents and the ^{13}C NMR spectroscopic chemical shifts are referenced to the ^{13}C signal(s) of the deuterated solvents. ^{19}F NMR spectroscopic chemical shifts are reported in ppm relative to CFCl$_3$ and referenced to an external solution of C_6F_6 in CDCl$_3$. ^{31}P NMR spectroscopic chemical shifts are reported in ppm relative to H_3PO_4 and referenced to an external 85% solution of phosphoric acid in D$_2$O. Abbreviations used in the description of NMR spectroscopic data are as follows: Ar=aryl, br=broad, v=virtual, s=singlet, d=doublet, m=multiplet.

Infrared spectra were recorded by using Nicolet Protégé 460 and Bruker Equinox 55 FTIR spectrometers. Electrospray ionization mass spectrometry (ESIMS) was performed at the Chemical Analysis Laboratory (Unit of Chemical Research Support) of the Weizmann Institute of Science, by using a Micromass Platform LCZ 4000 mass spectrometer (Micromass, Manchester, UK) with a cone voltage of 43 V, an extractor voltage of 4 V, and a desolvation temperature of 150°C.

Elemental analyses were performed at the Chemical Analysis Laboratory (Unit of Chemical Research Support) of the Weizmann Institute of Science and at H. Kolbe Mikroanalytisches Laboratorium, Mülheim an der Ruhr, Germany.

Crystal structures from the Cambridge structural database (CSD; version 5.29, November 2007),[43, 44] were retrieved and analyzed by using ConQuest v. 1.10[45] and Vista,[46] respectively. To avoid redundant crystal structures during the database search, we used the best representative polymorph list supplied by the Cambridge crystallographic data centre.[47] Analysis of short contacts in the crystal structures was performed with the free version of Mercury v. 1.4.[43, 48]

X-ray crystallographic analysis: Data were collected on a Nonius Kappa CCD diffractometer at 120(2) K (apart from one sample of *anti*-**3** that was also measured at 90(2) K), with Mo$_{K\alpha}$ radiation ($\lambda = 0.71073$ Å) and a graphite monochromator. Data processing was carried out by using Denzo-Scalepack.[49] Structures were solved by using direct methods in SHELXS-97 and refined in SHELXL-97 by using the full-matrix least-squares method based on F^2.[50]

Synthesis of complex 3: A solution of ligand **1** (100.7 mg, 0.402 mmol) in acetone (1.2 mL) was added to a solution of $[Rh(acetone)_2(coe)_2]BF_4$ (105.6 mg, 0.201 mmol) in acetone (1.1 mL), and the resulting solution was stirred at RT for 2 h. The orange-yellow solution was then concentrated under vacuum to 0.8 mL and added to a glass vial fitted with a rubber septum. CO gas was then freely bubbled through the solution by syringe for 1 min, then excess CO was pumped off. The resulting yellow

solution was filtered through a cotton pad and added with stirring to pentane (16 mL) to precipitate the product. The liquid phase was then decanted and the precipitate was washed with 4 mL of pentane and dried under vacuum. This gave the product as a yellow powder (115.0 mg, 0.154 mmol; 76.8 % yield).

^{1}H NMR (400 MHz, CD₂Cl₂): $\delta = 6.89$ (s, 4H; Ar), 3.29 (vt, ^2J(P,H) ≈ ^4J-(P,H) = 4.6 Hz, 4H; Ar−CH_2−P), 2.42 (m, 4H; PCH(CH₃)₂), 2.37 (s, 12H; Ar$_{ortho}$−CH_3), 2.24 (s, 6H; Ar$_{para}$−CH_3), 1.28 ppm (m, 24H; PCH(CH_3)₂); ^{13}C{^{1}H} NMR (101 MHz, CD₂Cl₂): $\delta = 186.74$ (dt, ^1J(Rh,C) = 64.7 Hz, ^2J-(P,C) = 13.7 Hz, CO), 138.23 (vt, J(P,C) = 1.8 Hz, C_{Ar}), 137.00 (vt, J(P,C) = 2.3 Hz, C_{Ar}), 130.55 (vt, J(P,C) = 1.2 Hz, C_{Ar}−H), 129.13 (s, C_{Ar}), 28.95 (vt, ^1J(P,C) ≈ ^3J(P,C) = 12.4 Hz, PCH(CH₃)₂), 24.62 (vt, ^1J(P,C) ≈ ^3J(P,C) = 10.9 Hz, Ar−CH₂−P), 22.46 (s, Ar$_{ortho}$−CH₃), 20.87 (s, Ar$_{para}$−CH₃), 19.58 (s, PCH(CH₃)₂), 19.13 ppm (s, PCH(CH₃)₂), peak assignment was confirmed by ^{13}C DEPT and ^{13}C−^{1}H heteronuclear correlation; ^{31}P{^{1}H} NMR (162 MHz, CD₂Cl₂): $\delta = 55.94$ ppm (d, ^1J(Rh,P) = 103.8 Hz); ^{19}F{^{1}H} NMR (376 MHz, CD₂Cl₂): $\delta = -153.33$ ppm (s, BF₄).

^{1}H NMR (400 MHz, CDCl₃): $\delta = 6.84$ (s, 4H; Ar), 3.28 (vt, ^2J(P,H) ≈ ^4J-(P,H) = 4.6 Hz, 4H; Ar−CH_2−P), 2.43 (m, 4H; PCH(CH₃)₂), 2.34 (s, 12H; Ar$_{ortho}$−CH_3), 2.22 (s, 6H; Ar$_{para}$−CH_3), 1.28 ppm (m, 24H; PCH(CH_3)₂); ^{31}P{^{1}H} NMR (162 MHz, CDCl₃): $\delta = 55.87$ ppm (d, ^1J(Rh,P) = 103.6 Hz); ^{19}F{^{1}H} NMR (376 MHz, CDCl₃): $\delta = -154.77$ ppm (s, BF₄).

^{1}H NMR (400 MHz, CD₃OD): $\delta = 6.91$ (s, 4H; Ar), 3.42 (vt, ^2J(P,H) ≈ ^4J-(P,H) = 4.6 Hz, 4H; Ar−CH_2−P), 2.52 (m, 4H; PCH(CH₃)₂), 2.41 (s, 12H; Ar$_{ortho}$−CH_3), 2.23 (s, 6H; Ar$_{para}$−CH_3), 1.31 (m, 24H; PCH(CH_3)₂); ^{31}P{^{1}H} NMR (162 MHz, CD₃OD): $\delta = 56.27$ ppm (d, ^1J(Rh,P) = 103.1 Hz).

IR (nujol): $\nu_{CO} = 2008$ cm⁻¹ (s); ESIMS (acetone/CH₃OH): m/z calcd for C₃₄H₅₄O₂P₂Rh: 659.27 [M]⁺; found: 660.19; m/z calcd for BF₄: 86.80 [M]⁻; found: 87.23; elemental analysis calcd. (%) for C₃₄H₅₄BF₄O₂P₂Rh: C 54.71, H 7.29; found: C 54.80, H 7.34.

X-ray structural analysis of *anti*-3 isolated from dioxane: Complex *anti*-3 was crystallized from dioxane at 95 °C.

Crystal Data: C₃₄H₅₄O₂P₂Rh·BF₄; $M_r = 746.43$; yellow prism; 0.4 × 0.3 × 0.3 mm³; triclinic; space group $P\bar{1}$; $a = 11.147(2)$ Å, $b = 12.297(3)$ Å, $c = 14.554(3)$ Å; $\alpha = 100.71(3)°$, $\beta = 107.37(3)°$, $\gamma = 99.82(3)°$; $V = 1815.7(6)$ Å³; $Z = 2$; $\rho_{calcd} = 1.365$ mg m⁻³, $\mu = 0.607$ mm⁻¹.

Solution and refinement: $R_{int} = 0.028$, 481 parameters with no restraints; final $R_1 = 0.0282$ (based on F^2) for data with $I > 2\sigma(I)$ and $R_1 = 0.0334$ for 8243 reflections; goodness of fit on $F^2 = 1.037$; largest electron density peak = 0.646 e Å⁻³.

X-ray structural analysis of *anti*-3 isolated from tetrahydrofuran: Complex *anti*-3 was crystallized from THF overlaid with pentane at −20 °C.

Crystal Data: C₃₄H₅₄O₂P₂Rh·BF₄; $M_r = 746.43$; yellow prism; 0.3 × 0.2 × 0.1 mm³; triclinic; space group $P\bar{1}$; $a = 11.146(2)$ Å, $b = 12.296(3)$ Å, $c = 14.541(3)$ Å; $\alpha = 100.68(3)°$, $\beta = 107.35(3)°$, $\gamma = 99.85(3)°$; $V = 1814.0(7)$ Å³; $Z = 2$; $\rho_{calcd} = 1.367$ mg m⁻³; $\mu = 0.608$ mm⁻¹.

Solution and refinement: $R_{int} = 0.065$, 475 parameters with no restraints; final $R_1 = 0.0441$ (based on F^2) for data with $I > 2\sigma(I)$ and $R_1 = 0.0547$ for 6968 reflections; goodness of fit on $F^2 = 1.044$; largest electron density peak = 0.844 e Å⁻³ and hole = −0.847 e Å⁻³.

X-ray structural analysis of *anti*-3 isolated from tetrahydrofuran, low temperature measurement (90 K): The crystal used for this measurement was prepared in the same way as the one described above (i.e., isolated from THF overlaid with pentane).

Crystal Data: C₃₄H₅₄O₂P₂Rh·BF₄; $M_r = 746.43$; yellow prism; 0.3 × 0.2 × 0.1 mm³; triclinic; space group $P\bar{1}$; $a = 11.117(2)$ Å, $b = 12.282(3)$ Å, $c = 14.534(3)$ Å; $\alpha = 100.68(3)°$, $\beta = 107.35(3)°$, $\gamma = 99.76(3)°$; $T = 90(2)$ K; $V = 1806.8(7)$ Å³; $Z = 2$; $\rho_{calcd} = 1.372$ mg m⁻³; $\mu = 0.610$ mm⁻¹.

Solution and refinement: $R_{int} = 0.058$, 475 parameters with no restraints; final $R_1 = 0.0393$ (based on F^2) for data with $I > 2\sigma(I)$ and $R_1 = 0.0547$ for 6972 reflections; goodness of fit on $F^2 = 1.043$; largest electron density peak = 0.597 e Å⁻³ and hole = −0.868 e Å⁻³.

X-ray structural analysis of *syn*-3 isolated from dichloromethane: Complex *syn*-3 was crystallized from dichloromethane overlaid with diethyl ether at −20 °C.

Crystal Data: C₃₄H₅₄O₂P₂Rh·BF₄·CH₂Cl₂; $M_r = 831.36$; yellow prism; 0.4 × 0.3 × 0.3 mm³; monoclinic; space group $P2_1/n$; $a = 17.910(4)$ Å, $b = 12.378(3)$ Å, $c = 19.731(4)$ Å; $\beta = 112.68(3)°$; $V = 4036(1)$ Å³; $Z = 4$; $\rho_{calcd} = 1.368$ mg m⁻³; $\mu = 0.682$ mm⁻¹.

Solution and refinement: $R_{int} = 0.051$, 500 parameters with no restraints; final $R_1 = 0.0420$ (based on F^2) for data with $I > 2\sigma(I)$ and $R_1 = 0.0570$ for 9199 reflections; goodness of fit on $F^2 = 1.063$; largest electron density peak = 1.302 e Å⁻³ and hole = −0.883 e Å⁻³.

H/D exchange experiment for complex 3 in CD₃OD: Complex 3 (6.7 mg, 0.009 mmol) was dissolved in CD₃OD (0.67 mL) and the resulting solution was placed in an NMR tube equipped with a rubber septum. CO gas was then freely bubbled through the solution for 1 min, then the septum was sealed with paraffin wax to avoid CO leakage. The ^{1}H and ^{31}P NMR spectra of this sample were recorded and then the solution was warmed at 80 °C for 17 d. ^{1}H and ^{31}P NMR spectra of the sample were recorded every few days and compared with the initial spectra. No significant changes were observed in the ^{31}P NMR spectrum, which indicated that no appreciable decomposition had taken place. This was corroborated by the ^{1}H NMR spectrum, in which essentially constant integral ratios were found between the residual C−H signal from the solvent, which was used as an internal standard, and all of the signals associated with 3, except for the signal associated with the arene methyl groups *ortho* to the methylene bridge. This signal was observed to disappear from the ^{1}H NMR spectrum during heating, which indicated that exchange of the respective protons with deuterons from the solvent had occurred.

Synthesis of complex 6: A solution of ligand 5 (47.2 mg, 0.113 mmol) in acetone (0.9 mL) was added to a solution of [Rh(acetone)₂(coe)₂]BF₄ (59.5 mg, 0.227 mmol) in acetone (1.1 mL) and the resulting solution was stirred at RT for 14 h. The red-orange solution was then added to a glass vial fitted with a rubber septum and CO gas was freely bubbled through the solution by syringe for 2 min with stirring. This resulted in rapid color change to orange-yellow. Excess CO was then pumped off and the solution was concentrated under vacuum to 0.8 mL. It was then added with stirring to pentane (18 mL) to precipitate the product. The liquid phase was decanted and the precipitate was washed with pentane and dried under vacuum, which gave the product as a yellow-orange powder (58.0 mg, 0.088 mmol, 77.9 % yield).

^{1}H NMR (400 MHz, CDCl₃): $\delta = 7.26$–7.20 (m, 10H; Ar), 3.43 (vt, ^2J-(P,H) ≈ ^4J(P,H) = 3.8 Hz, 4H; Ar−CH_2−P), 2.40 (m, ^3J(H,H) = 7.0 Hz, 4H; PCH(CH₃)₂), 1.23 ppm (m, 24H; PCH(CH_3)₂); ^{13}C{^{1}H} NMR (101 MHz, CDCl₃): $\delta = 187.87$ (dt, ^1J(Rh,C) = 64.8 Hz, ^2J(P,C) = 13.9 Hz, CO), 134.21 (vt, J(P,C) = 1.5 Hz, C_{Ar}), 129.93 (vt, J(P,C) = 2.5 Hz, C_{Ar}−H), 129.26 (s, C_{Ar}−H), 127.78 (vt, J(P,C) = 1.2 Hz, C_{Ar}−H), 30.68 (vt, ^1J(P,C) ≈ ^3J(P,C) = 11.2 Hz, Ar−CH₂−P), 26.83 (vt, ^1J(P,C) ≈ ^3J(P,C) = 12.8 Hz, PCH(CH₃)₂), 19.09 (s, PCH(CH₃)₂), 18.88 ppm (s, PCH(CH₃)₂), peak assignment was confirmed by ^{13}C DEPT; ^{31}P{^{1}H} NMR (162 MHz, CDCl₃): $\delta = 51.21$ ppm (d, ^1J(Rh,P) = 102.9 Hz); ^{19}F{^{1}H} NMR (376 MHz, CDCl₃): $\delta = -153.60$ ppm (br s, BF₄).

^{1}H NMR (400 MHz, CD₂Cl₂): $\delta = 7.38$–7.26 (m, 10H; Ar), 3.43 (vt, ^2J-(P,H) ≈ ^4J(P,H) = 3.8 Hz, 4H; Ar−CH_2−P), 2.43 (m, 4H; PCH(CH₃)₂), 1.29 ppm (m, 24H; PCH(CH_3)₂); ^{31}P{^{1}H} NMR (162 MHz, CD₂Cl₂): $\delta = 51.62$ ppm (d, ^1J(Rh,P) = 102.2 Hz).

^{1}H NMR (400 MHz, CD₃OD): $\delta = 7.43$–7.25 (m, 10H; Ar), 3.56 (vt, ^2J-(P,H) ≈ ^4J(P,H) = 3.0 Hz, 4H; Ar−CH_2−P), 2.50 (br m, 4H; PCH(CH₃)₂), 1.31 ppm (q, 24H; PCH(CH_3)₂); ^{31}P{^{1}H} NMR (162 MHz, CD₃OD): $\delta = 52.23$ ppm (br d, ^1J(Rh,P) = 103.3 Hz).

IR (nujol): $\nu_{CO} = 2015$ cm⁻¹ (s); ESIMS (CH₂Cl₂/CH₃OH): m/z calcd for C₂₈H₄₂O₂P₂Rh: 575.50 [M]⁺; found: 576.07; m/z calcd for C₂₇H₄₂OP₂Rh (complex−CO): 547.49 [M]⁺; found: 548.03; m/z calcd for BF₄: 86.80 [M]⁻; found: 87.23; elemental analysis calcd (%) for C₂₈H₄₂BF₄O₂P₂Rh: C 50.78, H 6.39; found: C 50.70, H 7.09.

X-ray structural analysis of 6 isolated from dichloromethane: Complex 6 was crystallized from dichloromethane overlaid with pentane at −20 °C.

Crystal Data: C₂₈H₄₂O₂P₂Rh·BF₄; $M_r = 662.28$; orange prism; 0.5 × 0.3 × 0.1 mm³; orthorhombic; space group $Pbcn$; $a = 15.9798(4)$ Å, $b = 11.6684(2)$ Å, $c = 16.5021(3)$ Å; $\alpha = \beta = \gamma = 90°$; $V = 3076.96(11)$ Å³; $Z = 4$; $\rho_{calcd} = 1.430$ mg m⁻³; $\mu = 0.707$ mm⁻¹.

Solution and refinement: $R_{int} = 0.044$, 213 parameters with no restraints; final $R_1 = 0.0348$ (based on F^2) for data with $I > 2\sigma(I)$ and $R_1 = 0.0844$ for 3852 reflections; goodness of fit on $F^2 = 0.934$; largest electron density peak $= 1.102$ e Å^{-3}.

X-ray structural analysis of 6 isolated from methanol: Complex **6** was crystallized from methanol overlaid with diethyl ether at $-20\,°C$.

Crystal Data: $C_{28}H_{42}O_2P_2Rh \cdot BF_4$; $M_r = 662.28$; orange prism; $0.3 \times 0.2 \times 0.2$ mm^3; orthorhombic; space group *Pbcn*; $a = 15.9820(3)$ Å, $b = 11.6800(5)$ Å, $c = 16.4920(3)$ Å; $\alpha = \beta = \gamma = 90°$; $V = 3078.56(15)$ Å^3; $Z = 4$; $\rho_{calcd} = 1.429$ mg m^{-3}; $\mu = 0.706$ mm^{-1}.

Solution and refinement: $R_{int} = 0.049$, 191 parameters with no restraints; final $R_1 = 0.0502$ (based on F^2) for data with $I > 2\sigma(I)$ and $R_1 = 0.0674$ for 2908 reflections; goodness of fit on $F^2 = 0.998$; largest electron density peak $= 2.418$ e Å^{-3}.

Reaction of 6 with CO—in situ preparation of 7: Complex **6** (13.7 mg, 0.021 mmol) was dissolved in CD$_2$Cl$_2$ (0.7 mL) and the resulting orange–yellow solution was added to a screw-cap NMR tube fitted with a rubber septum. CO gas was then freely bubbled through the solution by syringe for 2 min. The resulting yellow solution was then kept under a CO atmosphere during NMR spectra collection. The same procedure was also followed for a solution of **6** in CD$_3$OD.

^{1}H NMR (400 MHz, CD$_2$Cl$_2$): $\delta = 7.40$–7.33 (m, 6H; Ar), 7.19 (m, 4H; Ar), 3.41 (vt, ^2J(P,H) $\approx$ ^4J(P,H) $= 3.4$ Hz, 4H; Ar$-$C$H_2$$-$P), 2.43 (m, ^3J-(H,H) $= 7.0$ Hz, 4H; PCH(CH$_3$)$_2$), 1.39 (m, ^3J(H,H) $= 7.0$ Hz, 12H; PCH-(CH_3)$_2$), 1.32 ppm (m, ^3J(H,H) $= 7.0$ Hz, 12H; PCH(CH_3)$_2$); ^{13}C{^{1}H} NMR (101 MHz, CD$_2$Cl$_2$): $\delta = 186.10$ (br s, CO), 132.31 (vt, J-(P,C) $= 2.1$ Hz, C_{Ar}), 130.66 (vt, J(P,C) $= 2.2$ Hz, $C_{Ar}$$-$H), 129.59 (vt, J-(P,C) $= 1.1$ Hz, $C_{Ar}$$-$H), 128.62 (vt, J(P,C) $= 1.5$ Hz, $C_{Ar}$$-$H), 33.10 (vt, ^1J-(P,C) $\approx$ ^3J(P,C) $= 12.8$ Hz, Ar$-$C$H_2$$-$P), 27.96 (vt, ^1J(P,C) $\approx$ ^3J(P,C) $= 13.0$ Hz, PCH(CH$_3$)$_2$), 19.72 (s, PCH(CH_3)$_2$), 18.56 ppm (s, PCH(CH_3)$_2$), peak assignment was confirmed by ^{13}C DEPT; ^{31}P{^{1}H} NMR (162 MHz, CD$_2$Cl$_2$): $\delta = 62.69$ ppm (d, ^1J(Rh,P) $= 75.1$ Hz); ^{19}F{^{1}H} NMR (376 MHz, CD$_2$Cl$_2$): $\delta = -153.57$ ppm (s, BF$_4$).

^{1}H NMR (400 MHz, CD$_2$Cl$_2$, $-40\,°C$): $\delta = 7.36$–7.30 (m, 6H; Ar), 7.12 (m, 4H; Ar), 3.35 (vt, 4H; Ar$-$C$H_2$$-$P), 2.37 (m, 4H; PC$H$(CH$_3$)$_2$), 1.38 (m, 12H; PCH(C$H_3$)$_2$), 1.27 ppm (m, 12H; PCH(CH_3)$_2$); ^{13}C{^{1}H} NMR (101 MHz, CD$_2$Cl$_2$, $-40\,°C$): $\delta = 185.78$ (dt, ^1J(Rh,C) $= 66.4$ Hz, ^2J-(Rh,P) $= 13.7$ Hz, CO), 131.50 (vt, J(P,C) $= 2.2$ Hz, C_{Ar}), 130.40 (vt, J-(P,C) $= 1.7$ Hz, $C_{Ar}$$-$H), 129.18 (s, $C_{Ar}$$-$H), 128.24 (s, $C_{Ar}$$-$H), 32.82 (vt, ^1J-(P,C) $\approx$ ^3J(P,C) $= 13.3$ Hz, Ar$-$C$H_2$$-$P), 27.26 (vt, ^1J(P,C) $\approx$ ^3J(P,C) $= 13.1$ Hz, PCH(CH_3)$_2$), 19.64 (s, PCH(CH_3)$_2$), 17.77 ppm (s, PCH(CH_3)$_2$); ^{31}P{^{1}H} NMR (162 MHz, CD$_2$Cl$_2$, $-40\,°C$): $\delta = 64.30$ ppm (d, ^1J(Rh,P) $= 70.8$ Hz); ^{9}F{^{1}H} NMR (376 MHz, CD$_2$Cl$_2$, $-40\,°C$): $\delta = -153.07$ ppm (s, BF$_4$).

^{1}H NMR (400 MHz, CD$_3$OD): $\delta = 7.41$–7.25 (m, 10H; Ar), 3.57 (vt, ^2J-(P,H) $\approx$ ^4J(P,H) $= 3.5$ Hz, 4H; Ar$-$C$H_2$$-$P), 2.52 (m, 4H; PC$H$(CH$_3$)$_2$), 1.38 ppm (m, 24H; PCH(CH_3)$_2$); ^{31}P{^{1}H} NMR (162 MHz, CD$_3$OD): $\delta = 63.30$ ppm (d, ^1J(Rh,P) $= 72.6$ Hz).

IR (CH$_2$Cl$_2$): $\nu_{CO} = 2024$ (s), 2008 cm^{-1} (s).

Reaction of 6 with ^{13}CO—in situ preparation of ^{13}CO-labeled 7: Complex **6** (5.1 mg, 0.008 mmol) was dissolved in CDCl$_3$ (0.6 mL) and the resulting yellow solution was added to an NMR tube fitted with a rubber septum. A mixture of ^{13}CO and nitrogen was then freely bubbled through the solution by syringe for about 1 min, until the color changed to pale yellow. ^{1}H NMR (500 MHz, CDCl$_3$, $-50\,°C$): $\delta = 7.32$–7.27 (m, 6H; Ar), 7.08 (m, 4H; Ar), 3.38 (vt, 4H; Ar$-$C$H_2$$-$P), 2.42 (m, 4H; PC$H$(CH$_3$)$_2$), 1.40 (m, 12H; PCH(C$H_3$)$_2$), 1.29 ppm (m, 12H; PCH(CH_3)$_2$); ^{13}C{^{1}H} NMR (126 MHz, CDCl$_3$, $-50\,°C$): $\delta = 185.85$ (dt, ^1J(Rh,C) $= 66.2$ Hz, ^2J(Rh,P) $= 13.6$ Hz, CO), 131.41 (s, C_{Ar}), 130.42 (s, $C_{Ar}$$-$H), 129.26 (s, $C_{Ar}$$-$H), 128.38 (s, $C_{Ar}$$-$H), 32.92 (vt, ^1J(P,C) $\approx$ ^3J(P,C) $= 13.3$ Hz, Ar$-$C$H_2$$-$P), 27.25 (vt, ^1J(P,C) $\approx$ ^3J(P,C) $= 13.1$ Hz, PCH(CH_3)$_2$), 19.96 (s, PCH(CH_3)$_2$), 17.99 ppm (s, PCH(CH_3)$_2$); ^{31}P{^{1}H} NMR (202 MHz, CDCl$_3$, $-50\,°C$): $\delta = 64.33$ ppm (dq, ^1J(Rh,P) $= 70.5$ Hz, ^2J(C,P) $= 13.5$ Hz).

Computational details: All calculations were carried out by using Gaussian 03, Revision C.02.[51] We used the PBE0 DFT exchange-correlation functional,[52] also known as PBE1PBE. PBE0 is the hybrid variant of PBE, that is, Perdew, Burke, and Ernzerhof's nonempirical GGA func-

tional, and contains 25 % Hartree–Fock exchange. For the modeling of **4**, two basis set–RECP (relativistic effective core potential) combinations were used. The first, denoted SDD, is a combination of the Huzinaga–Dunning double-ζ basis set[53] for lighter elements and the Stuttgart–Dresden basis set–RECP combination[54] for transition metals. The second combination, denoted pc-1, combines Jensen's "polarization consistent" pc-1 basis set[55] for main-group elements and the Stuttgart–Dresden basis set–RECP combination[54] for transition metals with an added f-type polarization exponent taken as the geometric average of the two f-exponents given in the appendix of ref. [56] This combination is of double-ζ plus polarization quality. Model complexes *trans*-[Rh(CO)$_2$-(PH$_3$)$_2$]$^+$, *trans*-[Rh(CH$_4$)(CO)$_2$(PH$_3$)$_2$]$^+$ and *trans*-[Rh(CH$_4$)(CO)$_2$-(PMe$_3$)$_2$]$^+$ were treated at the PBE0/SDD level of theory. All structures have been fully optimized and characterized as energy minima by calculating the harmonic vibrational frequencies.

CCDC-671432–671435 contain the supplementary crystallographic data for **3** (three structures for the *anti* conformer, measured at two different temperatures, and one structure for the *syn* conformer). CCDC-689827 and -689828 contain crystallographic data for **6** (two structures). These data can be obtained free of charge from The Cambridge Crystallographic Data Centre via www.ccdc.cam.ac.uk/data_request/cif.

[1] J. A. Labinger, J. E. Bercaw, *Nature* **2002**, *417*, 507–514.

[2] K. Godula, D. Sames, *Science* **2006**, *312*, 67–72.

[3] M. Montag, L. Schwartsburd, R. Cohen, G. Leitus, Y. Ben-David, J. M. L. Martin, D. Milstein, *Angew. Chem.* **2007**, *119*, 1933–1936; *Angew. Chem. Int. Ed.* **2007**, *46*, 1901–1904.

[4] CO is usually regarded as a strong π-accepting ligand and is therefore expected to inhibit processes that increase the formal oxidation state of the metal center, such as oxidative addition.

[5] Ligand **1**, and various platinum and rhodium complexes thereof, has been previously reported by our group. For further details, see: a) M. van der Boom, S.-Y. Liou, L. J. W. Shimon, Y. Ben-David, D. Milstein, *Organometallics* **1996**, *15*, 2562–2568; b) M. van der Boom, J. Ott, D. Milstein, *Organometallics* **1998**, *17*, 4263–4266; c) M. Montag, G. Leitus, L. J. W. Shimon, Y. Ben-David, D. Milstein, *Chem. Eur. J.* **2007**, *13*, 9043–9055.

[6] For examples of analogous *trans*-dicarbonyl bisphosphine complexes of rhodium, see: a) G. K. N. Reddy, B. R. Ramesh, *J. Organomet. Chem.* **1974**, *67*, 443–447; b) A. R. Sedle, R. A. Newmark, R. D. Howells, *Inorg. Chem.* **1988**, *27*, 2473–2478; c) J. I. Dulebohn, S. C. Haefner, K. A. Berglund, K. R. Dunbar, *Chem. Mater.* **1992**, *4*, 506–508; d) E. Lindner, Q. Wang, H. A. Mayer, R. Fawzi, M. Steimann, *Organometallics* **1993**, *12*, 1865–1870; e) M. Alvarez, N. Lugan, B. Donnadieu, R. Mathieu, *Organometallics* **1995**, *14*, 365–370; f) E. T. Singewald, X. Shi, C. A. Mirkin, S. J. Schofer, C. L. Stern, *Organometallics* **1996**, *15*, 3062–3069; see also ref. [8].

[7] Crystal structures of rhodium complexes that contain terminal CO ligands in the *trans* configuration are quite rare. Our search of the Cambridge Structural Database (CSD, v. 5.29), which avoided redundant structures by being limited to the best representative polymorph list supplied by the Cambridge Crystallographic Data Centre, yielded 370 different crystal structures that contain the Rh(CO)$_2$ fragment (with R factor $\leq 10\%$, but no other constraints). Of these structures, only 12 (3 %) have a transoid configuration (165° $\leq$ $\measuredangle$ OC-Rh-CO $\leq 180°$), whereas the vast majority (355 structures, 96 %) have a cisoid configuration (80° $\leq$ $\measuredangle$ OC-Rh-CO $\leq 120°$). For

more information regarding CSD and the best representative polymorph list, see the Experimental Section.

[8] Only a handful of crystal structures of cationic *trans*-dicarbonyl bisphosphine Rh[I] complexes have been reported so far; for examples, see: a) S. C. Haefner, K. R. Dunbar, C. Bender, *J. Am. Chem. Soc.* **1991**, *113*, 9540–9553; b) O. Nurnberg, H. Werner, *J. Organomet. Chem.* **1993**, *460*, 163–175; c) L. Kirsten, G. Steyl, A. Roodt, *Acta Crystallogr. Sect. E* **2006**, *62*, m1702–m1704.

[9] The deviation of the C-Rh-C angle from linearity is not reflected in the IR spectrum of **3**, which features only one CO stretch band ($\tilde{\nu} = 2008\ \text{cm}^{-1}$) as described in the main text. However, this is to be expected, since for a C-Rh-C angle of 166° the intensity ratio of the asymmetric to symmetric CO stretch bands is estimated as $I_{asym}/I_{sym} \approx 66$ from the equation $I_{asym}/I_{sym} = \tan^2(\theta/2)$, in which θ is the angle between the CO vectors. Such a high intensity ratio renders the symmetric band practically undetectable.

[10] The best representative polymorph list of the CSD (v. 5.29) was found to contain a total of 24 969 different transition metal–carbonyl structures with terminal CO ligands, for which the *R* factor ≤ 10%. The vast majority of these structures (24 644, 99%) have angles of $173° \leq \not\angle\text{M-C-O} \leq 180°$, and only a minority (6395, 26%) have angles of $\not\angle\text{M-C-O} < 173°$. Moreover, out of the 21 311 transition metal–carbonyl structures that were found to contain M(CO)$_n$ ($n \geq 2$) fragments, the vast majority (20 556, 96%) have a cisoid configuration ($80° \leq \not\angle\text{C-M-C} \leq 120°$), whereas only a minority (5505, 27%) have a transoid configuration ($165° \leq \not\angle\text{C-M-C} \leq 180°$). Note that because most of the complexes in the polymorph list contain more than one M(CO)$_n$ ($n \geq 1$) fragment, there is considerable overlap in the different populations mentioned above and thus the total cited percentages can exceed 100%.

[11] The best representative polymorph list of the CSD (v. 5.29) was found to contain a total of 1063 different rhodium–carbonyl structures with terminal CO ligands, for which the *R* factor ≤ 10%. The vast majority of these structures (1024, 96%) have angles of $173° \leq \not\angle\text{Rh-C-O} \leq 180°$, and only 167 (16%) have angles of $\not\angle\text{Rh-C-O} < 173°$. Note that the majority of the latter structures (122 out of 167, or 73%) are clusters in which the rhodium center is bound to another metal atom.

[12] R. K. Hocking, T. W. Hambley, *Organometallics* **2007**, *26*, 2815–2823.

[13] K. P. Huber, G. Herzberg in *Molecular Spectra and Molecular Structure, Vol. IV: Constants of Diatomic Molecules*, Van Nostrand Reinhold, New York, **1979**.

[14] A short contact is defined as a nonbonding interatomic distance that is smaller than or equal to the sum of the van der Waals radii of the interacting atoms.

[15] Anagostic interactions, which have also been dubbed "preagostic" or "pregostic", span an M–H distance range of 2.3–2.9 Å. They are also characterized by an M-H-C angle range of 110–170°, into which the present case fits completely, with $\not\angle\text{Rh1-H13b-C13} = 153.9(14)°$ and $\not\angle\text{Rh1-H29c-C29} = 146.6(13)°$. For a concise overview of anagostic interactions, see: M. Brookhart, M. L. H. Green, G. Parkin, *Proc. Natl. Acad. Sci. USA* **2007**, *104*, 6908–6914.

[16] a) A. Albinati, C. G. Anklin, F. Ganazzoli, H. Rüegg, P. S. Pregosin, *Inorg. Chem.* **1987**, *26*, 503–508; b) A. Albinati, C. Arz, P. S. Pregosin, *Inorg. Chem.* **1987**, *26*, 508–513; c) W. I. Sundquist, D. P. Bancroft, S. J. Lippard, *J. Am. Chem. Soc.* **1990**, *112*, 1590–1596; d) M. Bortolin, U. Bucher, H. Reugger, L. M. Venanzi, A. Albinati, F. Lianza, *Organometallics* **1992**, *11*, 2514–2521; e) M. Cano, J. V. Heras, M. Maeso, M. Alvaro, R. Fernndez, E. Pinilla, J. A. Campo, A. Monge, *J. Organomet. Chem.* **1997**, *534*, 159–172; f) Y. Zhang, J. C. Lewis, R. G. Bergman, J. A. Ellman, E. Oldfield, *Organometallics* **2006**, *25*, 3515–3519.

[17] When a CD₃OD solution of **3** was warmed at 80°C for several days in a sealed NMR tube in the absence of added CO, partial decomposition was observed. Therefore, the H/D experiment described in the main text was conducted only after the solution had been purged with CO gas to obtain a CO-rich system, in an attempt to prevent this decomposition. Indeed, the ¹H NMR spectra indicated

that no significant decomposition had taken place during the prolonged heating period (17 d), with the residual C–H signal from the CD₃OD solvent being used as an internal standard. See the Experimental Section for more details.

[18] The extent of H/D exchange was estimated as 85% after 17 d at 80°C (based on integration of ¹H NMR signals; the ArC*H*₂P signal at 3.42 ppm was used as a reference). No significant H/D exchange was observed for the methyl groups *para* to the methylene bridge.

[19] The fact that the H/D exchange occurred at both *ortho* methyl groups of each ligand also supports the conclusion that the anagostic interactions alternate between the two methyl groups of each ligand, which is also evident from their magnetic equivalence in the ¹H NMR spectrum.

[20] All bond lengths and angles in the two structures are statistically equivalent, that is, the differences in each value lies within the 6σ (±3σ) limit.

[21] Diffraction data for the crystal isolated from THF were collected at two temperatures, 120 and 90 K, but no significant differences were found between the obtained crystal structures.

[22] The distance between C29 and the metal center in *syn*-**3** is 3.755(4) Å, which is not considered a short contact.

[23] The Rh−P bonds in *syn*-**3** (Rh1−P2 = 2.3498(9) Å, Rh1−P3 = 2.3548(8) Å) are slightly shorter than in *anti*-**3** (Rh1−P2 = 2.3626(10) Å, Rh1−P3 = 2.3699(11) Å).

[24] As far as the primary coordination sphere of rhodium is concerned, the calculated bond lengths for *anti*- and *syn*-**4** are within 1.2% of the experimentally observed values for *anti*- and *syn*-**3** (see Table 2). The calculated bond angles are within 3.5% of the experimental values, except for the C1-Rh-C2 angle in *syn*-**4**, which has a calculated value of 148.84° and is almost 10% smaller than the analogous angle in *syn*-**3** (164.70(11)°).

[25] The calculated values for the bond lengths associated with the anagostic interactions (Rh···H, Rh···C) are within 7.8% of the experimentally observed values (see Table 2).

[26] A partially covalent C−H···Rh interaction was also proposed by Bergman, Ellman, Oldfield, and co-workers for a planar cationic Rh[I] system (see ref. [16 f]). In their case, however, the interaction involved d$_{xz/yz}$ rather than d$_{z^2}$.

[27] M. Elian, R. Hoffmann, *Inorg. Chem.* **1975**, *14*, 1058–1076.

[28] R. Hoffmann, C. Minot, H. B. Gray1, *J. Am. Chem. Soc.* **1984**, *106*, 2001–2005.

[29] a) M. Ogasawara, S. A. Macgregor, W. E. Streib, K. Folting, O. Eisenstein, K. G. Caulton, *J. Am. Chem. Soc.* **1995**, *117*, 8869–8870; b) M. Ogasawara, S. A. Macgregor, W. E. Streib, K. Folting, O. Eisenstein, K. G. Caulton, *J. Am. Chem. Soc.* **1996**, *118*, 10189–10199.

[30] This complex also exhibited bent Ru-C-O angles of 168.2(8) and 168.7(7)°.

[31] Additional stabilization of the Ru⁰ system is attained by M-C-O bending, which reduces the σ donation from CO to d$_{yz}$ (see ref. [29]).

[32] The same conclusion was also made by Eisenstein, Caulton, and co-workers regarding the distorted CO−Ru−CO fragment in *trans*-[Ru(CO)₂(P*t*Bu₂Me)₂] (see ref. [29]).

[33] PMe₃ is a stronger donor than PH₃, and this is expected to increase the electron density on the metal center of [Rh(CH₄)(CO)₂(PMe₃)₂]⁺ relative to the PH₃ complex. If electrostatic interactions had been dominant in the C−H···Rh interaction, then the Rh···H distance would have been shorter in the more electron-rich system, contrary to the calculated results.

[34] The small energetic differences between the linear and bent structures (which are probably also associated with small energy barriers) and the labile C−H···Rh interactions lead to an inherently fluxional system that would be expected to exhibit averaged NMR signals.

[35] The shortest distance between the rhodium center and an arene C−H bond in the crystal structure of **6** is Rh1−H6 = Rh1−H6a = 3.13(3) Å.

[36] The linearity of the C1-Rh1-C1a and P2-Rh1-P2a angles in **6** is dictated by its C_i symmetry, that is, the fact that the center of inversion is located at the rhodium atom. Since C1 and C1a are symmetry-re-

lated, as are P2 and P2a, the error estimates for the above angles are equal to zero.

[37] The addition of CO to a CD₃OD solution of **6** was intended to stabilize the latter during an H/D exchange experiment, as done for **3**, because complex **6** was found to decompose upon warming to 80 °C in CD₃OD. However, the fact that **6** reacted with CO to afford **7** completely prevented us from using this H/D exchange technique for **6**.

[38] For examples of complexes of the type $[Rh(CO)_3(phosphine)_2]^+$, see: refs. [6f] and [8b], and F. M. Dixon, M. S. Masar III, P. E. Doan, J. R. Farrell, F. P. Arnold, Jr., C. A. Mirkin, C. D. Incarvito, L. N. Zakharov, A. L. Rheingold, *Inorg. Chem.* **2003**, *42*, 3245–3255.

[39] Further evidence for the reversibility of CO binding in **7** was obtained upon preparation of its ¹³CO-labeled analogue. As described in the Experimental Section, when a solution of nonlabeled **6** was treated with excess ¹³CO, the product, ¹³CO-labeled **7**, was found to contain only labeled CO. Because complex **6** is known to be stable under vacuum, it is likely that the replacement of CO ligands in **7** has occurred through dissociation of CO directly from **7**, rather than from **6**.

[40] B. Windmüller, O. Nürnberg, J. Wolf, H. Werner, *Eur. J. Inorg. Chem.* **1999**, 613–619. The procedure was modified by using AgBF₄ instead of AgPF₆ and conducting the whole process at room temperature.

[41] N. Holzhey, S. Pitter, *J. Mol. Catal. A* **1999**, *146*, 25–36.

[42] L. J. Farrugia, *J. Appl. Crystallogr.* **1997**, *30*, 565.

[43] Cambridge Crystallographic Data Centre, 12 Union Road, Cambridge, England.

[44] F. H. Allen, *Acta Crystallogr. Sect. B* **2002**, *58*, 380–388.

[45] I. J. Bruno, J. C. Cole, P. R. Edgington, M. Kessler, C. F. Macrae, P. McCabe, J. Pearson, R. Taylor, *Acta Crystallogr. Sect. B* **2002**, *58*, 389–397.

[46] *Vista*, A Program for the Analysis and Display of Data Retrieved from the CSD, Cambridge Crystallographic Data Centre, 12 Union Road, Cambridge (England), **1994**

[47] J. van de Streek, *Acta Crystallogr. Sect. B* **2006**, *62*, 567–579.

[48] C. F. Macrae, P. R. Edgington, P. McCabe, E. Pidcock, G. P. Shields, R. Taylor, M. Towler, J. van de Streek, *J. Appl. Crystallogr.* **2006**, *39*, 453–457.

[49] Z. Otwinowski, W. Minor, *Methods Enzymol.* **1997**, *276*, 307–326.

[50] G. M. Sheldrick, *Acta Crystallogr. Sect. A* **2008**, *64*, 112–122.

[51] Gaussian 03, Revision C.02, M. J. Frisch, G. W. Trucks, H. B. Schlegel, G. E. Scuseria, M. A. Robb, J. R. Cheeseman, J. A. Montgomery, T. Vreven, K. N. Kudin, J. C. Burant, J. M. Millam, S. S. Iyengar, J. Tomasi, V. Barone, B. Mennucci, M. Cossi, G. Scalmani, N. Rega, G. A. Petersson, H. Nakatsuji, M. Hada, M. Ehara, K. Toyota, R. Fukuda, J. Hasegawa, M. Ishida, T. Nakajima, Y. Honda, O. Kitao, H. Nakai, M. Klene, X. Li, J. E. Knox, H. P. Hratchian, J. B. Cross, V. Bakken, C. Adamo, J. Jaramillo, R. Gomperts, R. E. Stratmann, O. Yazyev, A. J. Austin, R. Cammi, C. Pomelli, J. W. Ochterski, P. Y. Ayala, K. Morokuma, G. A. Voth, P. Salvador, J. J. Dannenberg, V. G. Zakrzewski, S. Dapprich, A. D. Daniels, M. C. Strain, O. Farkas, D. K. Malick, A. D. Rabuck, K. Raghavachari, J. B. Foresman, J. V. Ortiz, Q. Cui, A. G. Baboul, S. Clifford, J. Cioslowski, B. B. Stefanov, G. Liu, A. Liashenko, P. Piskorz, I. Komaromi, R. L. Martin, D. J. Fox, T. Keith, M. A. Al-Laham, C. Y. Peng, A. Nanayakkara, M. Challacombe, P. M. W. Gill, B. Johnson, W. Chen, M. W. Wong, C. Gonzalez, J. A. Pople, Gaussian, Inc., Wallingford CT **2004**.

[52] J. P. Perdew, K. Burke, M. Ernzerhof, *Phys. Rev. Lett.* **1996**, *77*, 3865–3868.

[53] T. H. Dunning, Jr., P. J. Hay in *Modern Theoretical Chemistry, Vol. 3*, Plenum, New York, **1976**, pp. 1–28.

[54] "Effective Core Potentials": M. Dolg in *Modern Methods and Algorithms of Quantum Chemistry, Vol. 1*, John von Neumann Institute for Computing, Jülich (Germany), **2000**, pp. 479–508.

[55] F. Jensen, *J. Chem. Phys.* **2002**, *116*, 7372–7379.

[56] J. M. L. Martin, A. Sundermann, *J. Chem. Phys.* **2001**, *114*, 3408–3420.